bioRxiv preprint doi: https://doi.org/10.1101/2020.01.06.895813; this version posted January 7, 2020. The copyright holder for this preprint (which was not certified by peer review) is the author/funder, who has granted bioRxiv a license to display the preprint in perpetuity. It is made available under aCC-BY-NC 4.0 International license.

Electrochemical carbon fiber-based technique for simultaneous recordings of brain tissue PO_2, pH, and extracellular field potentials

Patrick S. Hosford[1,2*], Jack A. Wells[3], Isabel N. Christie[1], Mark Lythgoe[3], Julian Millar[4] and Alexander V. Gourine[1]

[1]*Centre for Cardiovascular and Metabolic Neuroscience, Neuroscience, Physiology & Pharmacology, University College London, London, UK*

[3]*Centre for Advanced Biomedical Imaging, Department of Medicine, University College London, London, UK*

[2]*William Harvey Research Institute, Barts and the London School of Medicine and Dentistry, London, UK*

[4]*Department of Medical Education, Barts and the London School of Medicine and Dentistry, London, UK*

*Corresponding author: PSH;

Email: p.hosford@ucl.ac.uk

Telephone: +440203182410

Address: Department of Neuroscience, Physiology & Pharmacology, University College London, Gower Street, London, UK, WC1E 6BT.

Abstract

A method for simultaneous electrochemical detection of brain tissue PO_2 (P_tO_2) and pH changes together with neuronal activity using a modified form of fast cyclic voltammetry with carbon fiber electrodes is described. This technique has been developed for *in vivo* applications and recordings from discrete brain nuclei in experimental animals. The small size of the carbon fiber electrode (⍰7µm, length <100µm) ensures minimal disruption of the brain tissue and allows recordings from small brain areas. Sample rate (up to 4 Hz) is sufficient to resolve rapid changes in P_tO_2 and pH that follow changes in neuronal activity and metabolism. Rapid switching between current and voltage recordings allows combined electrochemical detection and monitoring of extracellular action potentials. For simultaneous electrochemical detection of P_tO_2 and pH, two consecutive trapezoidal voltage ramps are applied with double differential-

bioRxiv preprint doi: https://doi.org/10.1101/2020.01.06.895813; this version posted January 7, 2020. The copyright holder for this preprint (which was not certified by peer review) is the author/funder, who has granted bioRxiv a license to display the preprint in perpetuity. It is made available under aCC-BY-NC 4.0 International license.

subtraction of the background current. This enables changes in current caused by protons and oxygen to be detected separately with minimal interference between the two. The profile of P_tO_2 changes evoked by increases in local neuronal activity recorded using the described technique was similar to that of blood oxygen level dependent responses recorded using fMRI. This voltammetric technique can be combined with fMRI and brain vessel imaging to study the metabolic mechanisms underlying neurovascular coupling response with much greater spatial and temporal resolution than is currently possible.

Keywords

Fast Cyclic voltammetry, carbon fiber electrode, tissue PO_2, pH, *in vivo*, extracellular potential, neurovascular coupling

Introduction

The method described here has been developed to study the mechanisms underlying the neurovascular coupling response (Hosford and Gourine 2018). The mechanisms of neurovascular coupling contribute to accurate matching of brain oxygen and glucose supply with demand. Sustained disruption of this balance has been postulated to contribute to cognitive impairment and the development of neurodegenerative disease (Iadecola 2017). Understanding the cellular and molecular mechanisms of neurovascular coupling could be important for the development of future treatments for these conditions. Yet, despite intense experimental scrutiny over the last two decades, the mechanisms underlying neurovascular coupling are not fully understood and are surrounded by controversies (Hosford and Gourine 2018).

The 'feed-forward' hypothesis of neurovascular coupling (Attwell et al. 2010) suggests that neurotransmitters released during neuronal activity signal to astrocytes and pericytes to induce dilation of the cerebral vasculature (Mishra et al. 2016). However, astrocytes are also sensitive to changes in partial pressure of oxygen (PO_2) (Angelova et al. 2015) as well as CO_2 and protons (H^+) (Gourine et al. 2010; Howarth et al. 2017; Karagiannis et al. 2016). Changes in brain tissue PO_2, PCO_2 and pH correlate with changes in neuronal activity and could

bioRxiv preprint doi: https://doi.org/10.1101/2020.01.06.895813; this version posted January 7, 2020. The copyright holder for this preprint (which was not certified by peer review) is the author/funder, who has granted bioRxiv a license to display the preprint in perpetuity. It is made available under aCC-BY-NC 4.0 International license.

contribute to neurovascular coupling via a metabolic feed-back mechanism, as was originally proposed by Roy and Sherrington (Roy and Sherrington 1890).

Blood oxygen level dependent functional magnetic resonance imaging (BOLD-fMRI) (Buxton and Frank 1997) and 2-photon excitation brain vessel imaging (Takano et al. 2006) have been widely used to study the mechanisms of the neurovascular response. However, these techniques have significant limitations. fMRI is non-invasive but suffers from relatively poor spatial and temporal resolution. This is particularly problematic in studies of the brain using small rodent models. Moreover, the BOLD fMRI signal represents a composite response determined by changes in blood flow, blood volume and oxygen consumption, and as such lacks specificity to the underlying haemodynamic mechanisms that give rise to functional hyperaemia. Direct and simultaneous recordings of neuronal activity, although notably achieved during fMRI in non-human primates by Logothetis and co-workers (Logothetis et al. 2001), are not routine. Optical brain imaging is usually confined to cortical structures with imaging depth limited by the light scattering properties of the tissue (Helmchen and Denk 2005). Additionally, to achieve simultaneous recordings of the vessel diameter and neuronal activity one must introduce calcium, voltage sensitive and/or cell specific dyes or genetically encoded sensors of activity. These come with their own caveats; for example there is evidence that commonly used calcium sensors also buffer intracellular calcium and may impair normal cellular function (Bootman et al. 2018). To overcome some of these issues we aimed to develop a minimally invasive technique for *in vivo* recordings of neuronal activity and associated metabolic changes with high spatial and temporal resolution.

Fast-cyclic voltammetry (FCV) using carbon fiber microelectrodes (CFM) is an established technique used to determine the dynamics of neurotransmitter release and reuptake *in vitro* and *in vivo* (Rodeberg et al. 2017). FCV relies on rapidly changing the potential of the CFM *vs* an $Ag/AgCl_2$ reference electrode several times a second over a narrow voltage range to oxidise or reduce the analyte of interest. The amplitude of the current flux between the CFM and the analyte is recorded and used to determine the analyte concentration. Specific advantages of this technique include the small electrode size making it ideal for studies of localised metabolic changes in small brain areas. There is minimal

bioRxiv preprint doi: https://doi.org/10.1101/2020.01.06.895813; this version posted January 7, 2020. The copyright holder for this preprint (which was not certified by peer review) is the author/funder, who has granted bioRxiv a license to display the preprint in perpetuity. It is made available under aCC-BY-NC 4.0 International license.

damage to the microcirculation within the tissue and the measurements can be confined to localised brain regions located at any depth. The sub-second time resolution of FCV allows detection of events that occur at the onset of neuronal activity and precede increases in blood flow (Logothetis et al. 2001). Separate electrochemical detection of tissue partial pressure of oxygen (PtO_2) and pH using FCV has been achieved previously (Bucher et al. 2014; Hosford et al. 2017; Takmakov et al. 2010). Here we describe a novel FCV-based technique that enables simultaneous recordings of key variables representing the metabolic state of the brain: brain tissue PO_2, pH and neuronal activity.

Materials and Methods

Carbon fiber microelectrodes

CFMs (diameter 7 µm) were made as described in detail previously (Hosford et al. 2015; Millar and Pelling 2001). Briefly, single carbon fiber monofilaments (Goodfellow Metals) of ~10cm in length were inserted into borosilicate glass tubing (1.5 mm O.D, Harvard Bioscience) pre-filled with acetone. After complete evaporation of the solvent, the glass tubing was transferred to a conventional horizontal micropipette puller (Model 97, Sutter Instruments) and heated to taper the glass under medium-fast pull speed. The carbon fiber bridging the two pulled electrodes was then cut and connected to a copper wire using a low-melting point tin-bismuth alloy. The carbon fiber tip was trimmed to ~80 µM in length by applying a high DC voltage source (~400 V) guided using a standard laboratory microscope.

Electrode Calibration

All the recordings were performed using the equipment detailed in Figure 1A. CFMs oxygen sensitivity calibration was performed in phosphate-buffered saline (PBS) containing (in mM) 137 NaCl, 2.7 KCl and 10 phosphate buffer (pH 7.4, unless otherwise stated) saturated with nitrogen to displace the dissolved oxygen. PO_2 of the solution was then increased stepwise by additions of PBS saturated with 100% oxygen and monitored using an optical oxygen sensor

bioRxiv preprint doi: https://doi.org/10.1101/2020.01.06.895813; this version posted January 7, 2020. The copyright holder for this preprint (which was not certified by peer review) is the author/funder, who has granted bioRxiv a license to display the preprint in perpetuity. It is made available under aCC-BY-NC 4.0 International license.

(Oxylite™; Oxford Optronix), adjusted for temperature. A calibration curve of electrode faradaic current changes vs PO_2 over a range of 5-75 mmHg was constructed.

pH calibration was performed in PBS adjusted to the desired pH using additions of HCL or NaOH and monitored using a standard pH meter. Electrodes were calibrated in a small volume (3 ml) bath that allowed rapid fluid exchange. From a starting point of pH 7.4, buffer pH was changed stepwise to either 7.6, 7.2 or 7.0 in a random order for a particular electrode. A calibration curve of electrode current changes over a pH range of 7.0-7.6 was constructed.

Ethical approval and animal husbandry

All animal experiments were performed in accordance with the European Commission Directive 2010/63/EU (European Convention for the Protection of Vertebrate Animals used for Experimental and Other Scientific Purposes) and the UK Home Office (Scientific Procedures) Act (1986) with project approval from the University College London Institutional Animal Care and Use Committee. The rats were obtained from Charles River UK and housed in a temperature-controlled room on a 12 h light/dark cycle. Animals had access to standard laboratory chow and water *ad libitum*. On completion of the experiments, the animals were humanely killed by an anaesthetic overdose (pentobarbital sodium, 60 mg kg^{-1}, i.v.).

Animal preparation

Adult male Sprague-Dawley rats (280-320g) were prepared for the experiments in accord with the previously established imaging protocols (Wells et al. 2015). Anaesthesia was induced by isoflurane (2.5-4.0% in oxygen-enriched air) to establish vascular access by femoral vein cannulation. Anaesthesia was then transitioned to α-chloralose (75 mg kg^{-1}, i.v. initial dose followed by supplementary doses of 10–20 mg kg^{-1}, i.v., as required). The right femoral artery was cannulated to monitor the arterial blood pressure. The trachea was cannulated and the animal was mechanically ventilated (~60 strokes min^{-1};

bioRxiv preprint doi: https://doi.org/10.1101/2020.01.06.895813; this version posted January 7, 2020. The copyright holder for this preprint (which was not certified by peer review) is the author/funder, who has granted bioRxiv a license to display the preprint in perpetuity. It is made available under aCC-BY-NC 4.0 International license.

stroke volume - 8 ml kg^{-1}) with oxygen-enriched room air using a positive pressure ventilator (Harvard Apparatus) or an MR-compatible small animal ventilator (CWE).

Arterial PO_2, PCO_2 and pH were recorded at regular intervals using a pH/blood gas analyser (Siemens) and maintained within the physiological ranges (PO_2 100–120 mmHg, CO_2 35–40 mmHg and pH at 7.35–7.45) by adjusting the frequency and/or volume of mechanical ventilation. Body temperature was maintained at 37.0±0.5°C

Fast scan cyclic voltammetry

After exposure of the skull surface by midline incision, access to the somatosensory cortex was established via a small craniotomy (~1 mm^2) The dura was pierced and reflected laterally to prevent damage to the microelectrode tip. Under the microscopic guidance and control of a micromanipulator, CFM was inserted into the somatosensory forelimb region of the cortex (S1FL; coordinates: 2.8-3.8 mm lateral, 1.3-1.5 caudal and 0.1-0.5 mm ventral from Bregma).

The CFM was slowly advanced and placed into the S1FL when clear evoked action potentials were recorded in response to the electrical stimulation (1 Hz) of the contralateral paw. The trapezoidal voltage ramps (Figure 1B) were applied to the CFM (2-4 Hz and 200 Vs^{-1} rate of voltage change.) The CFM signals were amplified (10x), passed through a 50 Hz noise eliminator (Digitimer), filtered to 500-5,000 Hz, digitised (Power1401; Cambridge Electronic Design) and recorded for offline isolation of faradaic currents corresponding to changes in $[H^+]$ and P_tO_2. Continuous switching between current and voltage recordings allowed near-simultaneous detection of the evoked potentials (voltage), $[H^+]$ and P_tO_2 changes (current). Electrical forelimb simulation was applied using a constant-current stimulator (Digitimer). Trains of stimulation (3 Hz, 1.5 mA, 300 µs pulse width) were applied 3 times per animal/experimental condition with intervals of at least 3 min between the stimulations. Neuronal responses were analysed by integration of the evoked volley of extracellular potentials with the baseline noise subtracted.

bioRxiv preprint doi: https://doi.org/10.1101/2020.01.06.895813; this version posted January 7, 2020. The copyright holder for this preprint (which was not certified by peer review) is the author/funder, who has granted bioRxiv a license to display the preprint in perpetuity. It is made available under aCC-BY-NC 4.0 International license.

Brainstem recordings

Animals were anaesthetised and instrumented as described above (Figure 1A). In this set of experiments the dorsal surface of the brainstem was exposed for CFM recordings as previously described (Hosford et al. 2015; Hosford et al. 2017). The left cervical vagus nerve was exposed, separated from the sympathetic trunk and placed on the bipolar silver wire electrodes for electrical stimulation (800 µA, 1 ms at 3 Hz).

fMRI

fMRI was performed using a 9.4T Agilent horizontal bore scanner (Agilent) as described in detail previously (Wells et al. 2015). Briefly, a 72 mm inner diameter volume coil was used for transmission and signal was received using a 4-channel array head coil (Rapid Biomedical). To assess T2* weighted BOLD signals the following sequence parameters were used: TR□=□5s, TI□=□2s, matrix size□=□64□×□64, FOV□=□35mm × 35mm, TE□=□10ms, single slice (slice thickness□=□2mm), inversion pulse bandwidth□=□20,000Hz (Hosford et al. 2018). BOLD responses in the S1FL region were triggered by electrical stimulation of the contralateral forelimb as described above.

Results and Discussion

Voltammetric recordings

Using the recoding setup illustrated in Figure 1A, two negatively-directed trapezoidal voltage ramps were applied to the CFM at an interval of 20 ms as illustrated in Figure 1Bi: the first from 0 to -0.5 V, the second from -0.5 to -1.0 V. Both voltage ramps generated a 'background' current due to the impedance of the electrode/ fluid interface (Figure 1Bii). The CFM currents generated during the ramps were digitised and the first was digitally subtracted from the second (Figure 1Biii). This produced a *differential background current,* (Figure 1Bvi)

bioRxiv preprint doi: https://doi.org/10.1101/2020.01.06.895813; this version posted January 7, 2020. The copyright holder for this preprint (which was not certified by peer review) is the author/funder, who has granted bioRxiv a license to display the preprint in perpetuity. It is made available under aCC-BY-NC 4.0 International license.

resulting from the *difference* between the currents on scans 1 and 2. This subtraction procedure was used to eliminate potential non-specific signals due to changes in tissue impedance, temperature, etc. These non-specific signals appear equally on both the scans and thus are removed by subtraction, allowing discrimination of changes that occur selectively on one or the other scan. Trapezoidal ramps were applied as the background current is predominantly capacitive, reducing this current to a low level during the flat part of the trapezoid where dV/dt is zero.

Using these recording parameters the electrode was found to generate a distinct current profile in response to changes in buffer pH or PO_2 (Figure 1C). Changes in $[H^+]$ caused changes in the CFM faradaic current in the voltage range between -0.1 to -0.3 V. These changes occurred only in the first of the two voltammetric scans and, therefore, were clearly present on the differential signal.

Oxygen is electrochemically reduced at a voltage between -0.5 and -1.0 V, generating a cathodal faradaic current. The current from oxygen reduction appears in the signal from the second (-0.5 to -1.0 V) ramp but not from the first ramp and thus could also be seen in the differential signal. Examples of the faradaic current changes in response to oxygen and pH changes in the buffer are illustrated in Figure 1C. There is a clear separation between the two peak currents allowing detection of changes in both analytes simultaneously with minimal interference between the two. Peak current changes are shown in Figure 1D.

Proposed detection mechanism

The proposed origin of the recorded faradic current is the pH dependent oxidation of the hydroquinone groups on the surface of the CFM (Runnels et al. 1999; Takmakov et al. 2010; Figure 1E). Our recordings support this hypothesis as distinct double-peaks of approximately the same voltage range are detected (Figure 1C). A third pH-dependent peak was reported by Takmakov and colleagues (Takmakov et al. 2010) and was ascribed to changes in electrode capacitance induced by protons disrupting the Helmholtz layer of charged water molecules surrounding the electrode tip and is, therefore, non-faradic in nature.

bioRxiv preprint doi: https://doi.org/10.1101/2020.01.06.895813; this version posted January 7, 2020. The copyright holder for this preprint (which was not certified by peer review) is the author/funder, who has granted bioRxiv a license to display the preprint in perpetuity. It is made available under aCC-BY-NC 4.0 International license.

Using double-differential waveform applied during sampling we were able to remove this effect of capacitance change (as it is present on both the waveforms) after subtraction of the resulting background current.

The reaction underlying oxygen detection is the reduction of oxygen to hydroxyl ions (Figure 1E). This reaction occurs in a series of steps involving the formation of intermediates, including hydrogen peroxide. It is non-reversible, as evident from a single unidirectional current peak on the voltammetry scan. There have been previous proposals for the mechanism of electrochemical reduction of oxygen on carbon surfaces (Taylor and Humffray 1975; Zimmerman and Wightman 1991). We propose the following mechanism (Scheme 1) which includes the formation of a hydroperoxyl intermediate as well as hydrogen peroxide.

CFM calibration

Relative CFM sensitivities to changes in pH and PO_2 were determined by construction of standard calibration curves in the expected physiological ranges of changes in both variables: 7.0-7.6 units of pH and 5-75 mmHg for PO_2. Peak faradaic current for pH detection was sampled at -200 mV on each of the scans. Current generated by oxygen was sampled once on each scan at 15 ms from the start of the flat phase of the trapezoid as at this time point the background current was minimal.

In vitro calibration demonstrated high CFM sensitivity to oxygen (1.1±0.1 nA per 10 mmHg PO_2; n= 10 electrodes) and protons (9.8 ± 0.8 nA per pH unit; n= 10 electrodes). Responses were linear within the physiological ranges of changes in these variables (PO_2, R^2=0.998; pH, R^2=0.981) (Figure 2A,B). Sensitivity to changes in oxygen did not change over the range of physiological pH values, nor the sensitivity to protons at different PO_2 levels (Figure 2D). Current responses to a 20 mmHg change in PO_2 were similar over a range of 7.0-7.6 units: 2.6±0.2 nA at pH 7.0, 2.6±0.2 nA at pH 7.2, 2.7±0.2 nA at pH 7.4 and 2.8±0.2 nA at pH 7.6. Current responses to 0.2 unit decreases in pH were similar over a 10-100 mmHg range of PO_2: 2.1±0.2 nA at 10 mmHg, 2.1±0.3 nA at 50 mmHg and 2.2±0.3 at 100 mmHg. There was minimal interference between the two

bioRxiv preprint doi: https://doi.org/10.1101/2020.01.06.895813; this version posted January 7, 2020. The copyright holder for this preprint (which was not certified by peer review) is the author/funder, who has granted bioRxiv a license to display the preprint in perpetuity. It is made available under aCC-BY-NC 4.0 International license.

measurements; PO_2-sensitive current was altered by a mere 0.003±0.005nA per 0.1 unit pH change, while pH-sensitive current changed by 0.1±0.03 nA per 10 mmHg change in PO_2 (n=6, Figure 2C and E).

These recordings show that there is no significant change in current produced by one analyte when the other varies over the physiological range expected in the brain tissue. Cross-talk between the pH and oxygen detection signals was calculated to be less than 5%, which is within the range reported for other electrochemical detection techniques (Tian et al. 2009). Further, we can confidently exclude potential contamination of the recorded signals by other oxidizable molecules as these require a positive waveform voltage, usually +1.3 V (Park et al. 2011), while this technique records PO_2 and pH changes using a negative (reducing) waveform of 0 to -1 V.

In vivo application

Using the recording setup illustrated by Figure 3A, changes in brain P_tO_2 were recorded during systemic hypoxia induced by a 20s-long suspension of the mechanical ventilation. This resulted in an immediate sharp decrease in oxygen-associated faradaic current by 3.2±0.6 nA, equivalent to a reduction in brain P_tO_2 by 19±3 mmHg (n=6; Figure 3Bi and ii). Upon re-instatement of lung ventilation, the brain P_tO_2 rapidly reversed and exceeded the baseline level by 15±4 mmHg within 10 s (n=6; Figure 3Bii).

Changes in brain P_tO_2 and pH were next recorded during systemic respiratory (hypercapnic) acidosis induced by CO_2 inhalation (10% CO_2 in the inspired gas mixture; 5 min). This stimulus caused a significant decrease in current by 0.31±0.05 nA (Figure 3Ci) in the voltage range corresponding to pH changes, equivalent to a decrease in brain tissue pH by -0.11±0.02 units (n=4; Figure 3Bii). Systemic hypercapnia also caused a 0.54±0.1nA increase in current (n=4; Figure 3Bii) over the voltage range corresponding to changes in PO_2, equivalent to an increase in brain P_tO_2 by 15±3 mmHg. This reflected CO_2-induced increase in global brain blood flow. Upon return to normocapnia the brain P_tO_2 decreased back to baseline within 3 min. Partial recovery of brain tissue pH was recorded during the same time period. The faradic current profiles recorded during

bioRxiv preprint doi: https://doi.org/10.1101/2020.01.06.895813; this version posted January 7, 2020. The copyright holder for this preprint (which was not certified by peer review) is the author/funder, who has granted bioRxiv a license to display the preprint in perpetuity. It is made available under aCC-BY-NC 4.0 International license.

systemic hypoxia and CO_2-induced acidosis were found to correspond closely to similar responses to changes in PO_2 and pH induced *in vitro*. Following subtraction of the control scan current from the active scan current, increases in oxygen concentration produce positive and increases in proton concentration produce negative current increments.

Electrical stimulation of the forepaw increased the neuronal activity in the S1FL of the cortex as was evident from an increase in action potential firing (recorded by the CFMs during the intervals between the applications of the voltage ramps; Figure 3D). Traces depicted in Figure 3D show the extracellular spike activity in S1FL, time-locked to the application of the stimulus.

Electrical stimulation of the forepaw was associated with a consistent increase in faradic current corresponding to an increase in P_tO_2 (n=6; Figure 3E). Increases in P_tO_2 were observed 1-2 seconds after the onset of the stimulation. The response was found to be biphasic with an initial increase during the period of stimulation followed by a post-stimulus decrease below the baseline (Figure 3E). Calibration of the CFM after each of the recordings revealed the peak increases in P_tO2 of 6.9±1.2mmHg and the post-stimulus decreases with the magnitude of 3.2±2.5 mmHg (n=6; Figure 3E). Activation of somatosensory pathways concomitantly increased the faradic current recorded at the sample point for the detection of pH changes. Changes in brain tissue extracellular pH followed a similar time course, but the pH response lagged the PO_2 changes by ~1 s. The pH signal displayed biphasic response profile with initial alkalisation of 0.06±0.02 pH units during the period of stimulation, followed by a decrease of 0.03±0.01 below baseline after the termination of the stimulus (n=6; Figure 3E).

There is evidence that the mechanisms of neurovascular coupling might be different in different brain areas (Devonshire et al. 2012). We next placed the CFM within the nucleus of the solitary tract (NTS) of the brainstem, and recorded changes in PtO_2 and pH evoked by activation of *visceral* sensory pathways. The NTS receives mono-synaptic afferent inputs via the vagus nerve (Berthoud and Neuhuber 2000). Electrical stimulation of the vagus nerve produced biphasic changes in both P_tO_2 and pH in the NTS that were markedly different from those

bioRxiv preprint doi: https://doi.org/10.1101/2020.01.06.895813; this version posted January 7, 2020. The copyright holder for this preprint (which was not certified by peer review) is the author/funder, who has granted bioRxiv a license to display the preprint in perpetuity. It is made available under aCC-BY-NC 4.0 International license.

recorded in the somatosensory cortex. There was an initial decrease in P_tO_2 by 4.5±2.2 mmHg and extracellular acidification by 0.095±0.04 pH units, followed by a post-stimulus overshoot in P_tO_2 by 2.3±0.9 mmHg (n=6; Figure 3F) with pH slowly recovering towards the baseline.

The P_tO_2 and pH recordings performed within the NTS show that this technique is applicable to studies of small discrete nuclei and/or regions located deep in the brain that are difficult to access using the existing imaging techniques. This could be especially useful when investigating the heterogeneity of the neurovascular coupling responses in the brain, as highlighted by dramatically different P_tO_2 and pH response profiles recorded in the NTS (Figure 3F) and the somatosensory cortex (Figure 3E).

Comparison with fMRI

BOLD signals induced in the S1FL by activation of somatosensory pathways were recorded in identical experimental conditions to allow comparison between the responses recorded using fMRI and P_tO_2 changes recorded using voltammetry. Electrical forepaw simulation induced biphasic BOLD signal changes in the S1FL (Figure 4A and B). In order to compare the BOLD signal changes with measured changes in P_tO_2, the calibrated voltammetry signal was down-sampled to 0.5Hz and both signals were standardised with a z-score function and overlaid (Figure 4C). Plotting the distance between each sample point for the two techniques revealed much of the difference observed during the post-stimulus undershoot, where it was maximal 6 s after the termination of the stimulus.

The data obtained show that the profile of brain PtO_2 changes recorded using this voltammetric technique is virtually identical to the profile of BOLD responses recorded using fMRI, with additional advantage of simultaneous detection of brain tissue pH and monitoring of the evoked neuronal activity.

Conclusion

Here we describe a novel experimental technique for simultaneous detection of brain P_tO_2, pH and extracellular field potentials using CFM voltammetry. Electrochemical detection of P_tO_2 and pH changes with near-simultaneous

bioRxiv preprint doi: https://doi.org/10.1101/2020.01.06.895813; this version posted January 7, 2020. The copyright holder for this preprint (which was not certified by peer review) is the author/funder, who has granted bioRxiv a license to display the preprint in perpetuity. It is made available under aCC-BY-NC 4.0 International license.

recordings of neuronal activity is possible in small nuclei located deep in the brain. Simultaneous monitoring of blood flow (P_tO_2), metabolism (pH) and neuronal activity using the CFM-based technique described here may prove to be useful in studies of the metabolic mechanisms underlying the neurovascular coupling response.

Acknowledgements

The author(s) disclose receipt of the following financial support for the research, authorship, and/or publication of this article:

This work was supported by The Wellcome Trust and British Heart Foundation

JAW is a Wellcome Trust/Royal Society Sir Henry Dale Fellow

AVG is a Wellcome Trust Senior Research Fellow (Refs: 095064 and 200893).

The author(s) declare no potential conflicts of interest with respect to the research, authorship, and/or publication of this article.

References

Angelova, P.R., Kasymov, V., Christie, I., Sheikhbahaei, S., Turovsky, E., Marina, N., Korsak, A., Zwicker, J., Teschemacher, A.G., Ackland, G.L., Funk, G.D., Kasparov, S., Abramov, A.Y., Gourine, A.V., 2015. Functional Oxygen Sensitivity of Astrocytes. J Neurosci 35(29), 10460-10473.

Attwell, D., Buchan, A.M., Charpak, S., Lauritzen, M., Macvicar, B.A., Newman, E.A., 2010. Glial and neuronal control of brain blood flow. Nature 468(7321), 232-243.

Berthoud, H.R., Neuhuber, W.L., 2000. Functional and chemical anatomy of the afferent vagal system. Auton Neurosci 85(1-3), 1-17.

Bootman, M.D., Allman, S., Rietdorf, K., Bultynck, G., 2018. Deleterious effects of calcium indicators within cells; an inconvenient truth. Cell Calcium 73, 82-87.

Bucher, E.S., Fox, M.E., Kim, L., Kirkpatrick, D.C., Rodeberg, N.T., Belle, A.M., Wightman, R.M., 2014. Medullary norepinephrine neurons modulate local oxygen concentrations in the bed nucleus of the stria terminalis. J Cereb Blood Flow Metab 34(7), 1128-1137.

bioRxiv preprint doi: https://doi.org/10.1101/2020.01.06.895813; this version posted January 7, 2020. The copyright holder for this preprint (which was not certified by peer review) is the author/funder, who has granted bioRxiv a license to display the preprint in perpetuity. It is made available under aCC-BY-NC 4.0 International license.

Buxton, R.B., Frank, L.R., 1997. A model for the coupling between cerebral blood flow and oxygen metabolism during neural stimulation. J Cereb Blood Flow Metab 17(1), 64-72.

Devonshire, I.M., Papadakis, N.G., Port, M., Berwick, J., Kennerley, A.J., Mayhew, J.E., Overton, P.G., 2012. Neurovascular coupling is brain region-dependent. Neuroimage 59(3), 1997-2006.

Gourine, A.V., Kasymov, V., Marina, N., Tang, F., Figueiredo, M.F., Lane, S., Teschemacher, A.G., Spyer, K.M., Deisseroth, K., Kasparov, S., 2010. Astrocytes control breathing through pH-dependent release of ATP. Science 329(5991), 571-575.

Helmchen, F., Denk, W., 2005. Deep tissue two-photon microscopy. Nat Methods 2(12), 932-940.

Hosford, P.S., Gourine, A.V., 2018. What is the key mediator of the neurovascular coupling response? Neurosci Biobehav Rev 96, 174-181.

Hosford, P.S., Millar, J., Ramage, A.G., 2015. Cardiovascular afferents cause the release of 5-HT in the nucleus tractus solitarii; this release is regulated by the low- (PMAT) not the high-affinity transporter (SERT). J Physiol 593(7), 1715-1729.

Hosford, P.S., Millar, J., Ramage, A.G., Marina, N., 2017. Abnormal oxygen homeostasis in the nucleus tractus solitarii of the spontaneously hypertensive rat. Exp Physiol 102(4), 389-396.

Hosford, P.S., Mosienko, V., Kishi, K., Jurisic, G., Seuwen, K., Kinzel, B., Ludwig, M.G., Wells, J.A., Christie, I.N., Koolen, L., Abdala, A.P., Liu, B.H., Gourine, A.V., Teschemacher, A.G., Kasparov, S., 2018. CNS distribution, signalling properties and central effects of G-protein coupled receptor 4. Neuropharmacology 138, 381-392.

Howarth, C., Sutherland, B., Choi, H.B., Martin, C., Lind, B.L., Khennouf, L., LeDue, J.M., Pakan, J.M., Ko, R.W., Ellis-Davies, G., Lauritzen, M., Sibson, N.R., Buchan, A.M., MacVicar, B.A., 2017. A Critical Role for Astrocytes in Hypercapnic Vasodilation in Brain. J Neurosci 37(9), 2403-2414.

Iadecola, C., 2017. The Neurovascular Unit Coming of Age: A Journey through Neurovascular Coupling in Health and Disease. Neuron 96(1), 17-42.

Karagiannis, A., Sylantyev, S., Hadjihambi, A., Hosford, P.S., Kasparov, S., Gourine, A.V., 2016. Hemichannel-mediated release of lactate. J Cereb Blood Flow Metab 36(7), 1202-1211.

Logothetis, N.K., Pauls, J., Augath, M., Trinath, T., Oeltermann, A., 2001. Neurophysiological investigation of the basis of the fMRI signal. Nature 412(6843), 150-157.

Millar, J., Pelling, C.W., 2001. Improved methods for construction of carbon fibre electrodes for extracellular spike recording. J Neurosci Methods 110(1-2), 1-8.

Mishra, A., Reynolds, J.P., Chen, Y., Gourine, A.V., Rusakov, D.A., Attwell, D., 2016. Astrocytes mediate neurovascular signaling to capillary pericytes but not to arterioles. Nat Neurosci 19(12), 1619-1627.

Park, J., Takmakov, P., Wightman, R.M., 2011. In vivo comparison of norepinephrine and dopamine release in rat brain by simultaneous measurements with fast-scan cyclic voltammetry. J Neurochem 119(5), 932-944.

Rodeberg, N.T., Sandberg, S.G., Johnson, J.A., Phillips, P.E., Wightman, R.M., 2017. Hitchhiker's Guide to Voltammetry: Acute and Chronic Electrodes for in Vivo Fast-Scan Cyclic Voltammetry. ACS Chem Neurosci 8(2), 221-234.

Roy, C.S., Sherrington, C.S., 1890. On the Regulation of the Blood-supply of the Brain. J Physiol 11(1-2), 85-158 117.

bioRxiv preprint doi: https://doi.org/10.1101/2020.01.06.895813; this version posted January 7, 2020. The copyright holder for this preprint (which was not certified by peer review) is the author/funder, who has granted bioRxiv a license to display the preprint in perpetuity. It is made available under aCC-BY-NC 4.0 International license.

Runnels, P.L., Joseph, J.D., Logman, M.J., Wightman, R.M., 1999. Effect of pH and surface functionalities on the cyclic voltammetric responses of carbon-fiber microelectrodes. Anal Chem 71(14), 2782-2789.
Takano, T., Tian, G.F., Peng, W., Lou, N., Libionka, W., Han, X., Nedergaard, M., 2006. Astrocyte-mediated control of cerebral blood flow. Nat Neurosci 9(2), 260-267.
Takmakov, P., Zachek, M.K., Keithley, R.B., Bucher, E.S., McCarty, G.S., Wightman, R.M., 2010. Characterization of local pH changes in brain using fast-scan cyclic voltammetry with carbon microelectrodes. Anal Chem 82(23), 9892-9900.
Taylor, R.J., Humffray, A.A., 1975. Electrochemical studies on glassy carbon electrodes: II. Oxygen reduction in solutions of high pH (pH>10). Journal of Electroanalytical Chemistry and Interfacial Electrochemistry 64(1), 63-84.
Tian, F., Gourine, A.V., Huckstepp, R.T., Dale, N., 2009. A microelectrode biosensor for real time monitoring of L-glutamate release. Anal Chim Acta 645(1-2), 86-91.
Wells, J.A., Christie, I.N., Hosford, P.S., Huckstepp, R.T., Angelova, P.R., Vihko, P., Cork, S.C., Abramov, A.Y., Teschemacher, A.G., Kasparov, S., Lythgoe, M.F., Gourine, A.V., 2015. A critical role for purinergic signalling in the mechanisms underlying generation of BOLD fMRI responses. J Neurosci 35(13), 5284-5292.
Zimmerman, J.B., Wightman, R.M., 1991. Simultaneous electrochemical measurements of oxygen and dopamine in vivo. Anal Chem 63(1), 24-28.

Figure Legends

Figure 1: Electrochemical detection of PO_2 and pH changes using carbon fiber microelectrodes (CFM). **A.** Schematic diagram of the required equipment for simultaneous electrochemical and electrophysiological recordings using CFM. *Left*: construction of carbon-in-glass CFM. *Right*: a block diagram of electrochemical signal generation and acquisition. A voltage driver combined with current amplifier is used for the electrochemical signal generation and detection. A voltage amplifier is used to record neuronal activity between applications of electrochemical waveform. Recorded signal is filtered by a standard band pass filter. All signals are digitised online and recorded for offline analysis. **B**. Electrochemical signal generation and processing: i) two inverted trapezoidal drive voltage waveforms applied to the electrode; the first from 0 to -0.5 V and the second from -0.5 to -1 V. ii) Background current profile generated by the voltage waveform resulting from the capacitive nature of the electrode. iii) Shows the background current resulting from the two applied voltage waveforms combined by superimposition; the resulting combined background current is stored digitally and vi) subtracted from the subsequently

bioRxiv preprint doi: https://doi.org/10.1101/2020.01.06.895813; this version posted January 7, 2020. The copyright holder for this preprint (which was not certified by peer review) is the author/funder, who has granted bioRxiv a license to display the preprint in perpetuity. It is made available under aCC-BY-NC 4.0 International license.

acquired scans to provide the measure of the current generated by changes in analyte concentration at the surface of the electrode. **C.** False color plots illustrating current changes over the voltage range of the electrochemical waveform cycling from 0 to -1 V recorded in phosphate-buffered saline. *Left* shows the current changes induced by a reduction in buffer pH from 7.4 to 6.8 units. *Right* shows the current changes induced by an increase in buffer PO_2 from 0 to 50 mmHg. Sample points when the peak current changes were measured are indicated for pH and PO_2. **D**. Representative recordings of CFM electrochemical current changes in response to given changes in pH and PO_2. **E**. Proposed detection schemes for protons (*left*) and oxygen (*right*) during the voltammetric scan on the surface of the CFM. Protonation of quinone groups on the surface of the CFM produces the current associated with the pH changes. Oxygen is reduced via intermediate steps to hydroxide. The flux of electrons from the CFM to molecular oxygen produces the current associated with changes in PO_2.

Figure 2: Validation of the technique and calibration of CFMs. **A.** Calibration curve illustrating changes in CFM electrochemical current recorded at the pH sample point in response to changes in buffer pH from 7.4 to 7.0, 7.2 and 7.6. Calibration points represent the means (±S.E.M) peak current changes of 10 electrodes exposed to a given change in buffer pH starting from 7.4. **B.** Calibration curve illustrating changes in CFM electrochemical current recorded at the oxygen sample point in response to changes in buffer PO_2 between 5-75 mmHg. Calibration points represent the means (±S.E.M) peak current changes of 10 electrodes, each exposed to every PO_2 increment once. Standard linear regression was applied to fit a line for both calibrations; the equation and R^2 are indicated. **C.** Representative traces showing changes in peak current at the PO_2 and pH sample points during a decrease in buffer pH of 0.2 units or increase in buffer PO_2 by 50 mmHg. **D.** *Left*: summary data showing peak currents generated in response to a 20 mmHg increase in PO_2 over a physiological range of changes in buffer pH at 7.0, 7.2, 7.4 or 7.6 units. Each point represents the mean (±S.E.M) peak response of 12 electrodes. *Right*: summary data showing peak currents generated in response to a 0.2 unit decrease in pH over a physiological range of changes in PO_2 at: 10, 50 and 100 mmHg. Each point represents the mean (±S.E.M) peak response of 9 electrodes. **E.** Summary data

bioRxiv preprint doi: https://doi.org/10.1101/2020.01.06.895813; this version posted January 7, 2020. The copyright holder for this preprint (which was not certified by peer review) is the author/funder, who has granted bioRxiv a license to display the preprint in perpetuity. It is made available under aCC-BY-NC 4.0 International license.

of peak current changes recorded at the pH and PO_2 sample points in response to a decrease in pH by 0.2 units (*left*) and at the pH and PO_2 sample points in response to an increase in PO_2 by 50 mmHg (*right*). Shown are the means (±S.E.M) peak current responses of 6 electrodes.

Figure 3: Simultaneous detection of brain tissue PO_2, pH, and extracellular field potentials. **A.** Schematic illustration of the *in vivo* recording setup in an anesthetised rat showing placement of the CFM in the somatosensory cortex with Ag/AgCl reference electrode in the contralateral hemisphere. The forepaw was stimulated electrically to recruit somatosensory pathways. Separate placement of the CFM in the nucleus of the solitary tract (NTS) and the vagus nerve stimulator are also shown. **B.** The effect of apnoea on oxygen-sensitive current recorded in the somatosensory cortex. i) False color plot showing changes in oxygen-sensitive current over the range of the voltammetric scan during a 20 s apnoeic episode. The sample point from which the oxygen-sensitive current was recorded is indicated. ii) Brain P_tO_2 changes recorded using CFM during systemic hypoxia (means±S.E.M; n=6) **C.** The effect of respiratory acidosis induced by inhalation of 10% CO_2 in the inspired gas mixture on oxygen and proton-sensitive currents recorded in the somatosensory cortex. i) False color plot showing changes in oxygen and proton-sensitive currents over the range of the voltammetric scan during systemic hypercapnia. The sample points from which the oxygen and proton-sensitive currents were recorded are indicated. ii) Brain tissue PO_2 and pH changes recorded using CFM during systemic hypercapnia (means±S.E.M; n=4) **D.** Representative recording of extracellular field potentials in the somatosensory cortex evoked by electrical forelimb stimulation during simultaneous brain P_tO_2 and pH sampling. *Inset* illustrates the intervals between pH/PO_2 sampling available for extracellular potential recording. **E.** Changes in brain P_tO_2 and pH recorded in the somatosensory cortex in response to electrical forelimb stimulation (3 Hz, 20 s; means ±S.E.M; n=6). **F.** Changes in P_tO_2 and pH recorded in the nucleus of the solitary tract of the brainstem in response to electrical stimulation of the vagus nerve (3 Hz, 20 s; means ±S.E.M; n=6).

Figure 4: Comparison of brain P_tO_2 changes profile recorded using CFM voltammetry and that of BOLD responses recorded using fMRI. **A.** BOLD

bioRxiv preprint doi: https://doi.org/10.1101/2020.01.06.895813; this version posted January 7, 2020. The copyright holder for this preprint (which was not certified by peer review) is the author/funder, who has granted bioRxiv a license to display the preprint in perpetuity. It is made available under aCC-BY-NC 4.0 International license.

response profile illustrating changes in mean signal intensity in the somatosensory cortex (S1FL) induced by the electrical stimulation of the contralateral forelimb in anesthetised rats (means ± S.E.M; n=6). **B.** Representative BOLD activation map (familywise error, p < 0.05, nv = 3) taken at one coronal slice (distance from Bregma is indicated) level showing activation of the somatosensory cortex in an anesthetised rat. Color bar represents the t-score from statistical parametric mapping mixed-effects analysis, p < 0.05 (uncorrected). **C.** Comparison of time course and response profile of standardised P_tO_2 and BOLD responses in the S1FL of the anesthetised rat evoked by forelimb simulation. Responses are represented as a mean z-score from the recordings obtained in 6 animals for each experimental measurement. The standard difference is the difference calculated between the two z-scores at each sample point. P_tO_2 recordings were down sampled by averaging 8 sampled data points to achieve the sampling frequency of 0.5 Hz, equal to that of the fMRI sampling rate.

Scheme 1: Proposed intermediate and overall reaction scheme underlying the reduction of molecular oxygen on the carbon surface.

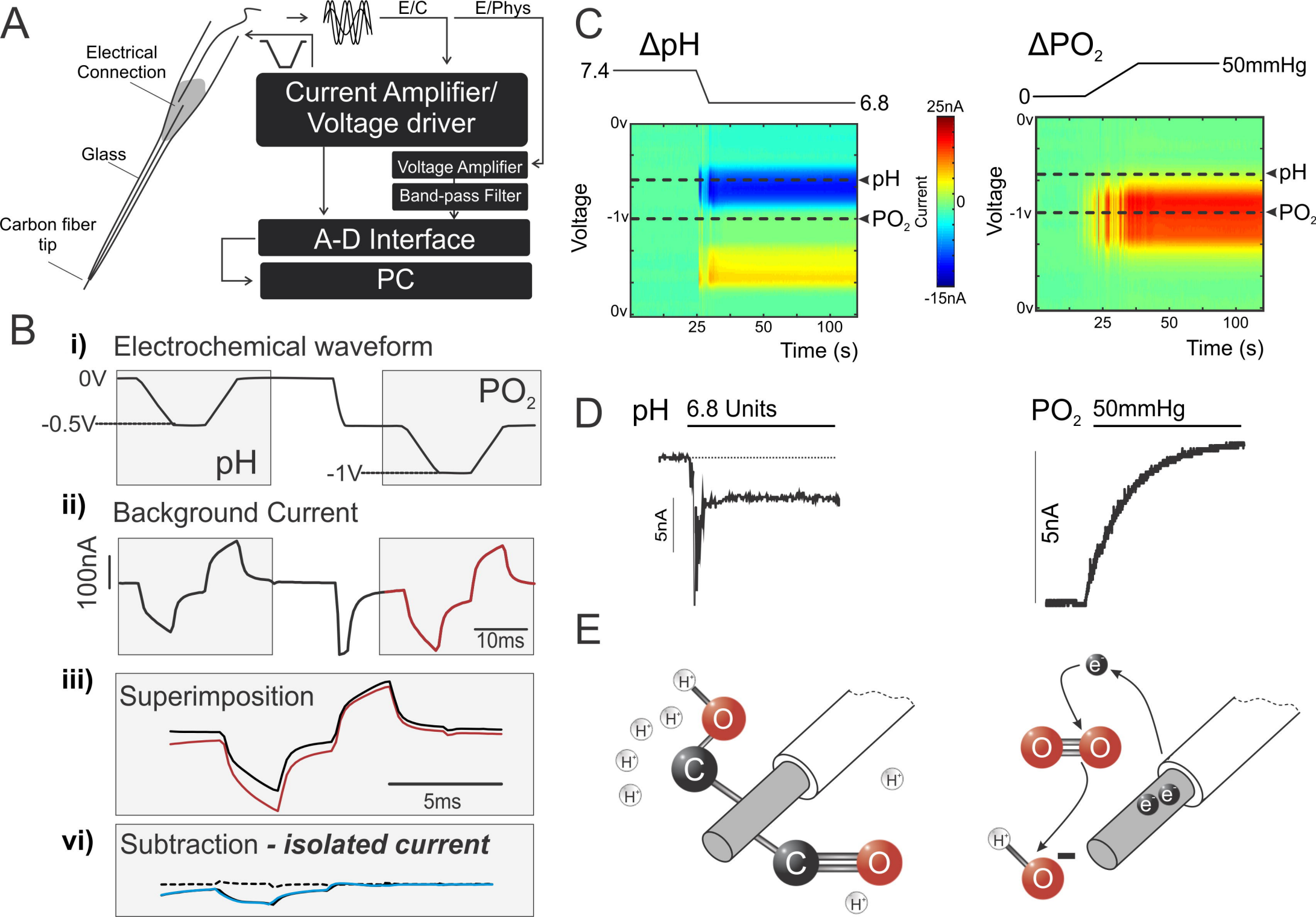
A
Electrical Connection
Glass
Carbon fiber tip
E/C
E/Phys
Current Amplifier/ Voltage driver
Voltage Amplifier
Band-pass Filter
A-D Interface
PC
B
i) Electrochemical waveform
0V
-0.5V
pH
PO2
-1V
ii) Background Current
100nA
10ms
iii) Superimposition
5ms
vi) Subtraction - isolated current
C
ΔpH
7.4
6.8
0v
-1v
0v
Voltage
pH
PO2
25nA
Current
0
-15nA
25
50
100
Time (s)
ΔPO2
0
50mmHg
0v
-1v
0v
Voltage
pH
PO2
25
50
100
Time (s)
D
pH 6.8 Units
5nA
PO2 50mmHg
5nA
E
H+
O
C
C
O
H+
e-
O
O
e-
e-
H+
O

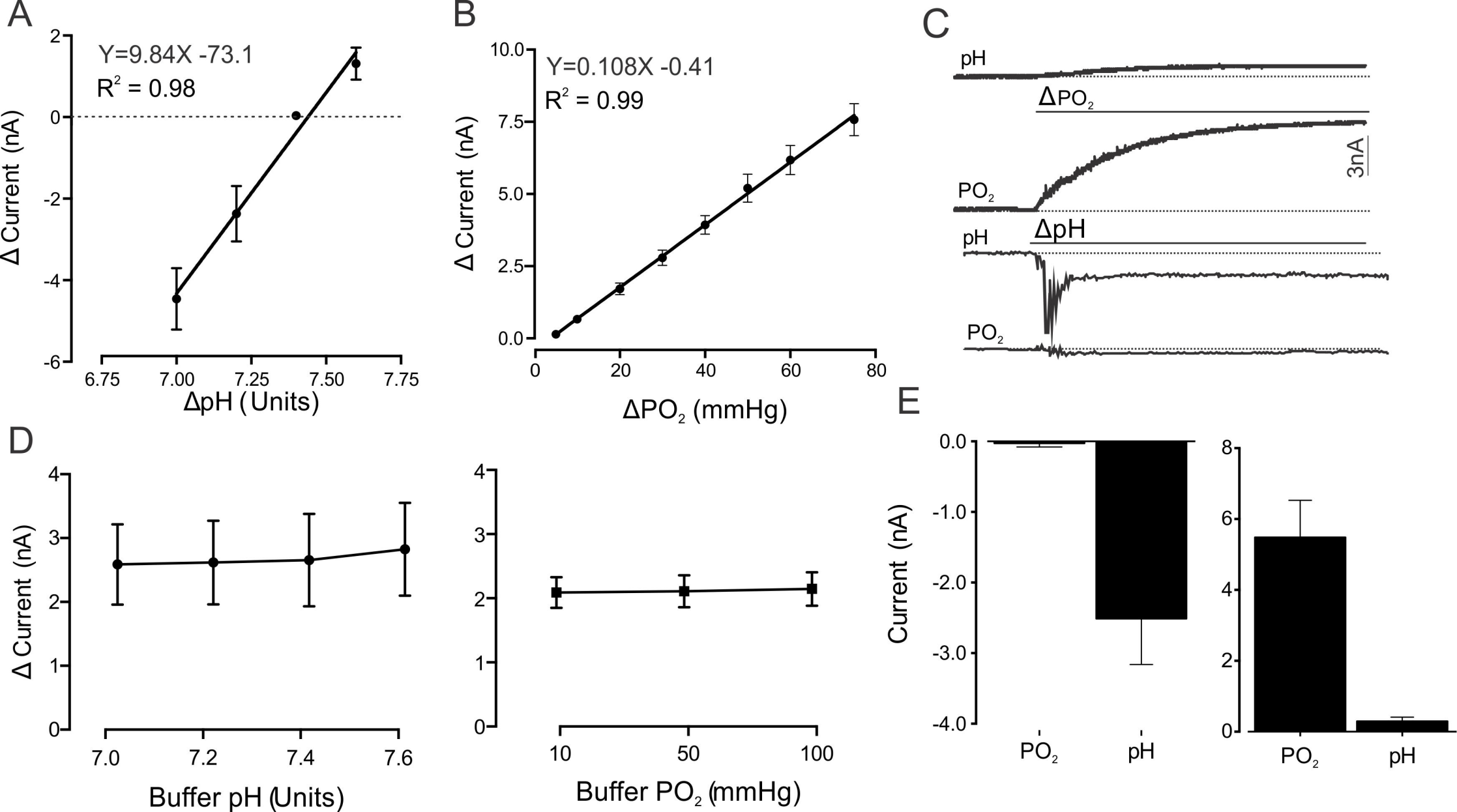
A
Y=9.84X -73.1
R² = 0.98
Δ Current (nA)
ΔpH (Units)
B
Y=0.108X -0.41
R² = 0.99
Δ Current (nA)
ΔPO₂ (mmHg)
C
pH
ΔPO₂
3nA
PO₂
pH
ΔpH
PO₂
D
Δ Current (nA)
Buffer pH (Units)
Buffer PO₂ (mmHg)
E
Current (nA)
PO₂
pH
PO₂
pH

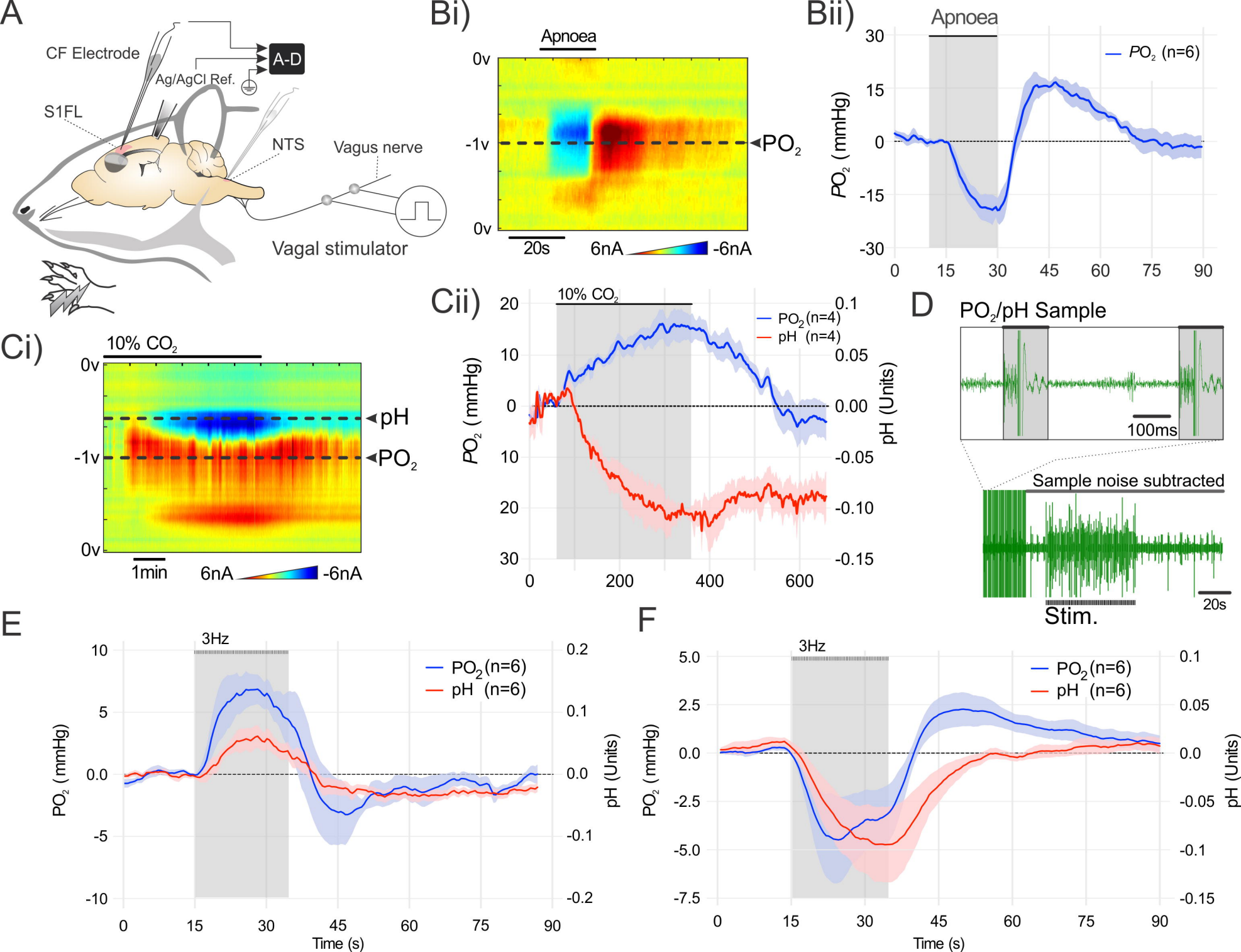
A
CF Electrode
A-D
Ag/AgCl Ref.
S1FL
NTS
Vagus nerve
Vagal stimulator
Bi)
Apnoea
0v
-1v
0v
PO2
20s
6nA
-6nA
Bii)
Apnoea
PO2 (n=6)
PO2 (mmHg)
30
15
0
-15
-30
0
15
30
45
60
75
90
Ci)
10% CO2
0v
-1v
0v
pH
PO2
1min
6nA
-6nA
Cii)
10% CO2
PO2 (n=4)
pH (n=4)
PO2 (mmHg)
pH (Units)
20
10
0
10
20
30
0.1
0.05
0.00
-0.05
-0.10
-0.15
0
200
400
600
D
PO2/pH Sample
100ms
Sample noise subtracted
20s
Stim.
E
3Hz
PO2 (n=6)
pH (n=6)
PO2 (mmHg)
pH (Units)
10
5
0.0
-5
-10
0.2
0.1
0.0
-0.1
-0.2
0
15
30
45
60
75
90
Time (s)
F
3Hz
PO2 (n=6)
pH (n=6)
PO2 (mmHg)
pH (Units)
5.0
2.5
0.0
-2.5
-5.0
-7.5
0.1
0.05
0.0
-0.05
-0.1
-0.15
0
15
30
45
60
75
90
Time (s)

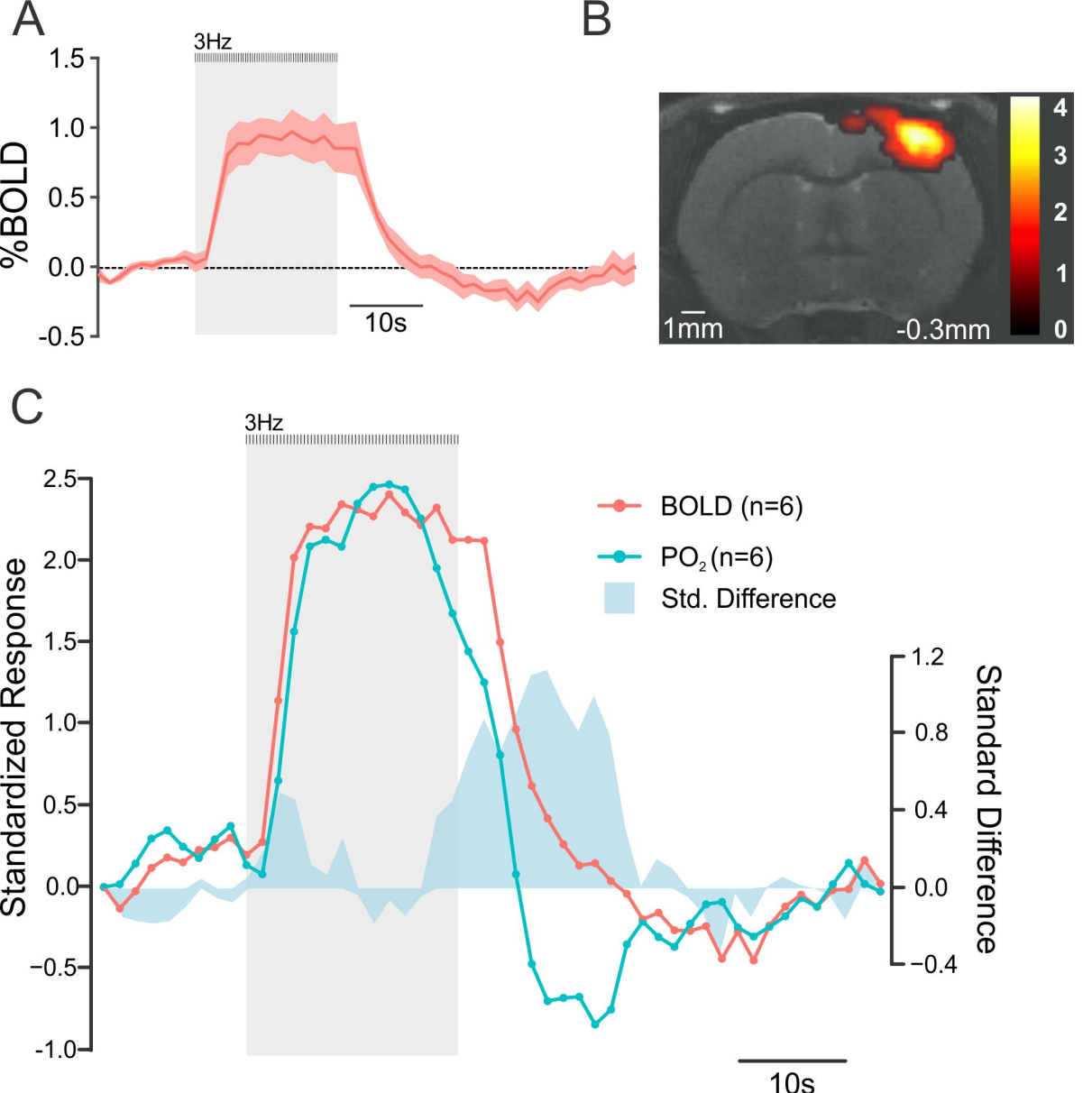
A
3Hz
1.5
1.0
0.5
0.0
-0.5
%BOLD
10s
B
4
3
2
1
0
1mm
-0.3mm
C
3Hz
2.5
2.0
1.5
1.0
0.5
0.0
-0.5
-1.0
Standardized Response
BOLD (n=6)
PO2 (n=6)
Std. Difference
1.2
0.8
0.4
0.0
−0.4
Standard Difference
10s

Scheme 1

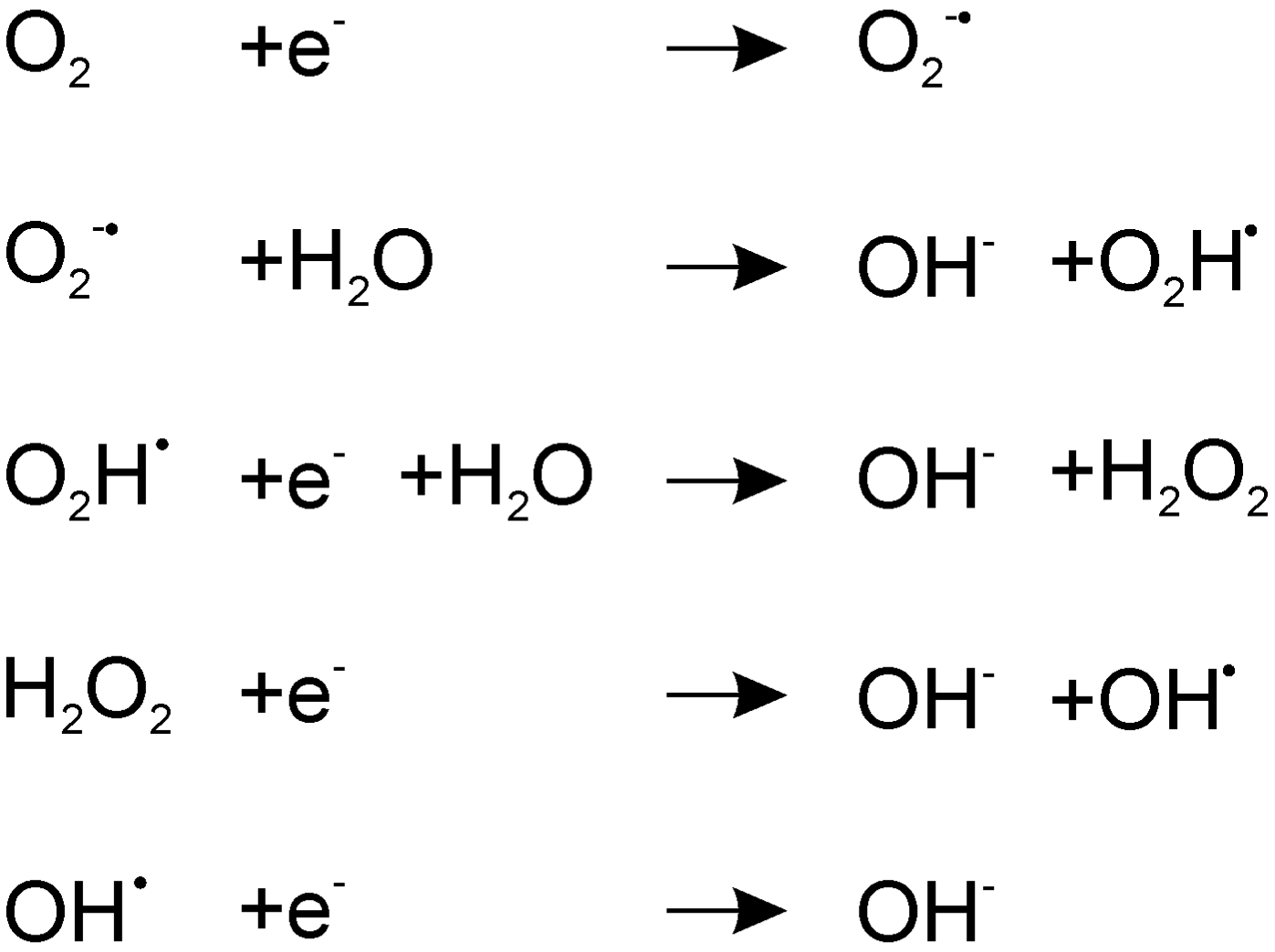

$$O_2 + 2H_2O + 4e^- \longrightarrow 4OH^-$$

overall reaction